JACS
JOURNAL OF THE AMERICAN CHEMICAL SOCIETY
pubs.acs.org/JACS
Article

# Site-Differentiated $Mn^{II}Fe^{II}$ Complex Reproducing the Selective Assembly of Biological Heterobimetallic Mn/Fe Cofactors

Anna L. Poptic, Ying-Pin Chen, Tieyan Chang, Yu-Sheng Chen, Curtis E. Moore, and Shiyu Zhang*

Cite This: J. Am. Chem. Soc. 2023, 145, 3491−3498
Read Online
ACCESS | Metrics & More | Article Recommendations | Supporting Information



**ABSTRACT:** Class Ic ribonucleotide reductases (RNRIc) and R2-like ligand-binding oxidases (R2lox) are known to contain heterobimetallic $Mn^{II}Fe^{II}$ cofactors. How these enzymes assemble $Mn^{II}Fe^{II}$ cofactors has been a long-standing puzzle due to the weaker binding affinity of $Mn^{II}$ versus $Fe^{II}$. In addition, the heterobimetallic selectivity of RNRIc and R2lox has yet to be reproduced with coordination complexes, leading to the hypothesis that RNRIc and R2lox overcome the thermodynamic preference for coordination of $Fe^{II}$ over $Mn^{II}$ with their carefully constructed three-dimensional protein structures. Herein, we report the selective formation of a heterobimetallic $Mn^{II}Fe^{II}$ complex accomplished in the absence of a protein scaffold. Treatment of the ligand $Py_4DMcT$ (**L**) with equimolar amounts of $Fe^{II}$ and $Mn^{II}$ along with two equivalents of acetate (OAc) affords $[LMn^{II}Fe^{II}(OAc)_2(OTf)]^+$ ($\mathbf{Mn^{II}Fe^{II}}$) in 80% yield, while the diiron complex $[LFe^{II}Fe^{II}(OAc)_2(OTf)]^+$ ($\mathbf{Fe^{II}Fe^{II}}$) is produced in only 8% yield. The formation of $\mathbf{Mn^{II}Fe^{II}}$ is favored regardless of the order of addition of $Fe^{II}$ and $Mn^{II}$ sources. X-ray diffraction (XRD) of single crystals of $\mathbf{Mn^{II}Fe^{II}}$ reveals an unsymmetrically coordinated carboxylate ligand—a primary coordination sphere feature shared by both RNRIc and R2lox that differentiates the two metal binding sites. Anomalous XRD studies confirm that $\mathbf{Mn^{II}Fe^{II}}$ exhibits the same site selectivity as R2lox and RNRIc, with the $Fe^{II}$ ($d^6$) center preferentially occupying the distorted octahedral site. We conclude that the successful assembly of $\mathbf{Mn^{II}Fe^{II}}$ originates from (1) Fe-deficient conditions, (2) site differentiation, and (3) the inability of ligand **L** to house a dimanganese complex.

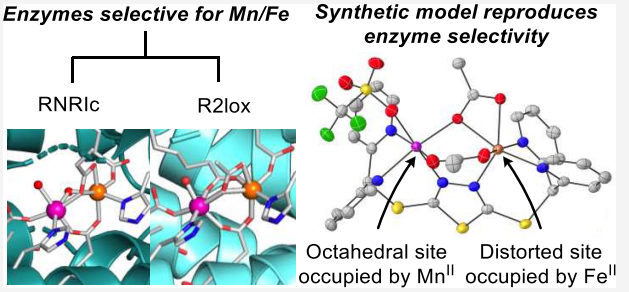


## INTRODUCTION

Heterobimetallic cofactors have been discovered in a number of proteins responsible for life-sustaining chemical transformations, including the heme $a_3/Cu_B$ site in cytochrome *c* oxidase, [NiFe] hydrogenase, Cu/Zn superoxide dismutase, and the Mn/Fe or Zn/Fe sites in purple acid phosphatases.[1] Mn/Fe cofactors have also been characterized in class Ic ribonucleotide reductases (RNRIc),[2−9] R2-like ligand-binding oxidases (R2lox),[10−25] and, most recently, in the chlamydia protein associated with death domains (CADD).[26] Since their discovery, heterobimetallic cofactors have piqued the interest of chemists and biologists alike. Understanding the mechanisms behind metallocofactor assembly can aid in answering important questions regarding protein evolution and metal selectivity in native and engineered proteins.[27−29]

Of the heterobimetallic cofactors, the most intriguing are those that incorporate $Mn^{II}$ and $Fe^{II}$—two metal ions of similar size and binding affinity—with apparent selectivity.[30] Despite sharing similar coordination environments to the diiron sites in canonical bacterial multicomponent monooxygenases (BMMs),[31−34] both RNRIc and R2lox feature distinct, site-selective heterobimetallic Mn/Fe cofactors (Figure 1A).[6,19,20]

The mechanism of heterobimetallic $Mn^{II}Fe^{II}$ cofactor assembly *in vivo* has been the subject of intense scrutiny. Work by Högbom et al.,[12,13,19−25] Shafaat et al.,[14−17] Stubbe et al.,[3−5] and Bollinger et al.[6−9] suggests that favorable $Mn^{II}Fe^{II}$ assembly is likely driven by a combination of metal availability and differential binding affinity. While *in vivo* studies have provided valuable insights into the selective formation of $Mn^{II}Fe^{II}$ cofactors, the complexity of the protein matrix has prevented the identification of specific structural features responsible for this process.

As studies on the assembly of RNRIc and R2lox continue, there have also been a number of attempts to replicate the primary coordination sphere, site differentiation, and selectivity of RNRIc and R2lox with coordination compounds.[35−49] However, the synthesis of $Mn^{II}Fe^{II}$ species is often complicated by simultaneous formation and/or scrambling of the heterobimetallic complex to form homobimetallic $Fe^{II}Fe^{II}$ and $Mn^{II}Mn^{II}$ analogues (Figure 1B).[38,39] To synthesize pure Mn/Fe complexes, pioneering work by Que et al. employed iron(III)/manganese(II) sources, along with a stepwise

Received: November 9, 2022
Published: February 7, 2023

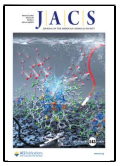




https://doi.org/10.1021/jacs.2c11930
J. Am. Chem. Soc. 2023, 145, 3491−3498

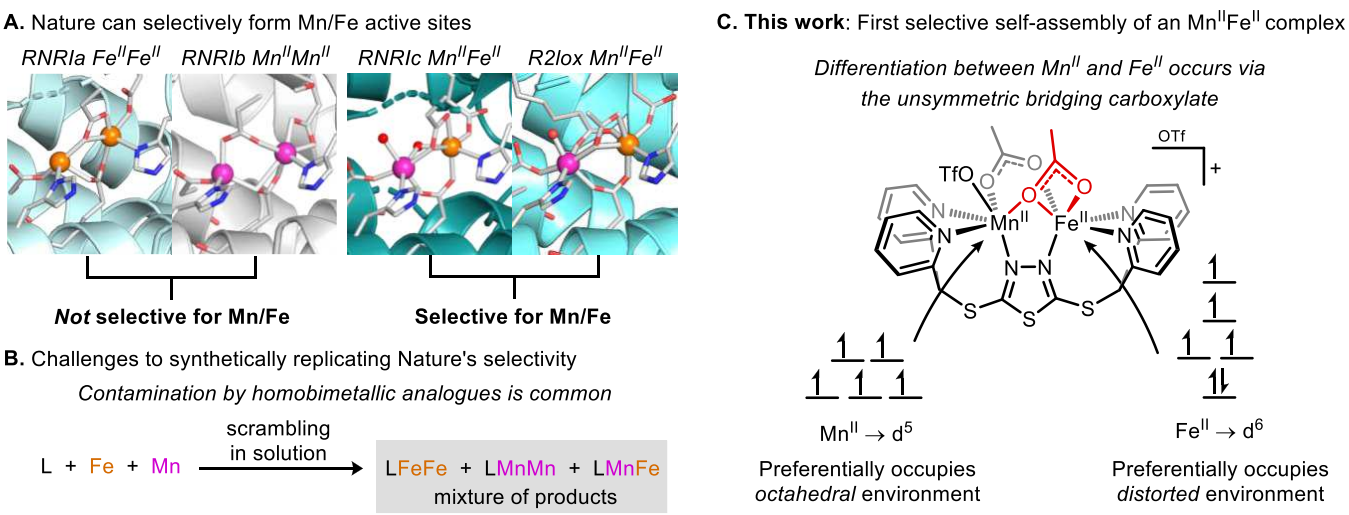


**Figure 1.** (A) Pymol rendered active sites of class Ia ribonucleotide reductase (PDB: 1PIY), Ib (PDB: 6TQW), Ic (PDB: 4M1I), and R2lox (PDB: 4HR4). (B) Scrambling of heterobimetallic complexes to form homobimetallic complexes. (C) Site-differentiated $Mn^{II}Fe^{II}$ complex in this work.

synthetic route to differentiate the binding event of each metal (Figure 2A).[35,44] A second synthetic strategy was developed by Wieghardt/Girerd et al., in which the heterobimetallic species was formed via self-assembly from two independently synthesized mononuclear complexes (Figure 2B).[36,43] Following these early studies, Neves et al.,[45] Chaudhuri et al.,[46] Blondin/Latour et al.,[48] Borovik et al.,[40,49] and Lu et al.[38] have utilized ligands with unsymmetric coordination environments to further bias the coordination of each metal to inequivalent sites (Figure 2C,D).

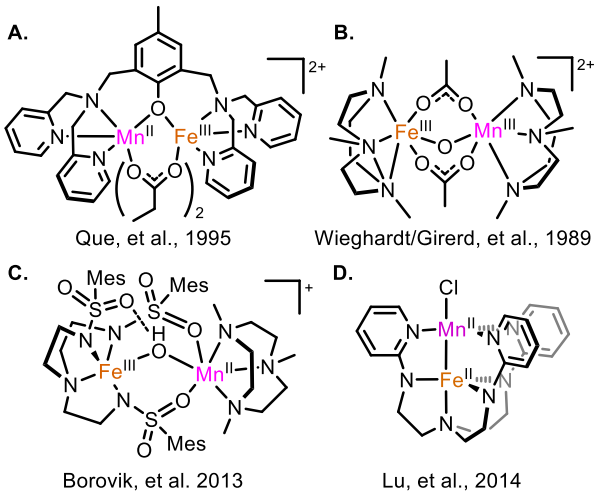


**Figure 2.** (A–D) Previously reported synthetic Mn/Fe complexes.

While previous synthetic studies have greatly increased our understanding of Mn/Fe complex formation, none have been able to shed light on the formation of MnFe cofactors under biologically relevant conditions, i.e., self-assembly in the presence of both Mn and Fe sources at a II,II state. Within the primary coordination spheres of RNRIc and R2lox, the only feature that differentiates the two metal binding sites is an unsymmetric $\mu$-1,1 bridging carboxylate residue. The unsymmetric binding mode of the carboxylate leads to distinct geometries at each site: an octahedral site that preferentially binds $Mn^{II}$ and a distorted octahedral site that primarily binds $Fe^{II}$ (Figure 1A).[6,19,20]

Herein, we report the first synthetic $Mn^{II}Fe^{II}$ complex containing an unsymmetric $\mu$-1,1 bridging acetate ligand. Despite the lack of a protein scaffold, the $Mn^{II}Fe^{II}$ complex self-assembles in the presence of both $Fe^{II}$ and $Mn^{II}$ (Figure 1C). Regardless of the order of $Fe^{II}$ and $Mn^{II}$ addition to the ligand $Py_4DMcT$, the heterobimetallic complex remains the major product with >72% selectivity. Anomalous X-ray diffraction (XRD) studies confirm that the $Mn^{II}Fe^{II}$ model complex has the same site selectivity as R2lox and RNRIc, where $Mn^{II}$ occupies the octahedral site and $Fe^{II}$ occupies the distorted site. The structural similarities of our model complex to R2lox and RNRIc, along with the same metal site selectivity, allow us to propose a mechanism for heterobimetallic $Mn^{II}Fe^{II}$ formation that does not contradict the classical Irving–Williams series.

## RESULTS AND DISCUSSION

**Synthesis and Characterization.** To design a ligand capable of supporting a Mn/Fe bimetallic center, we modified our previous $Py_4DMB$ system[50,51] by introducing a dimercaptan-1,3,4-thiadiazole linker. The new ligand **L** was synthesized in 85% yield ($Py_4DMcT$, **L**; Scheme 1). Treatment of **L** with one equivalent each of bis-acetonitrile iron(II) triflate ($Fe^{II}(OTf)_2MeCN_2$) and iron(II) acetate ($Fe^{II}(OAc)_2$) in a 1:1 mixture of chloroform/methanol, followed by recrystallization from dichloromethane/ether, affords orange crystals of $[LFe^{II}_2(OAc)_2(OTf)][OTf]$ (**$Fe^{II}Fe^{II}$**) in 70% yield (Scheme 2, left). We found that the heterobimetallic analogue can be synthesized by replacing $Fe^{II}(OTf)_2MeCN_2$ with one equivalent of bis-acetonitrile manganese(II) triflate ($Mn^{II}(OTf)_2MeCN_2$) (Scheme 1, left). Recrystallization from dichloromethane/ether results in yellow crystals of $[LMn^{II}Fe^{II}(OAc)_2(OTf)][OTf]$ (**$Mn^{II}Fe^{II}$**) in 60% yield (Figure 2B). Single-crystal XRD analysis reveals that both **$Fe^{II}Fe^{II}$** and **$Mn^{II}Fe^{II}$** contain two bridging acetate anions with symmetric and unsymmetric $\mu$-1,3/$\mu$-1,1 binding modes, respectively (Scheme 2). Despite being isostructural, **$Fe^{II}Fe^{II}$** and **$Mn^{II}Fe^{II}$** crystallize with different unit cell parameters (Figure 3A,B; see the Supporting Information). The M–M separation in **$Mn^{II}Fe^{II}$** (3.4794(6) Å) is also slightly longer


https://doi.org/10.1021/jacs.2c11930
J. Am. Chem. Soc. 2023, 145, 3491–3498

**Scheme 1. Synthesis of $Py_4DMcT$ (L) and Metal Complexes**

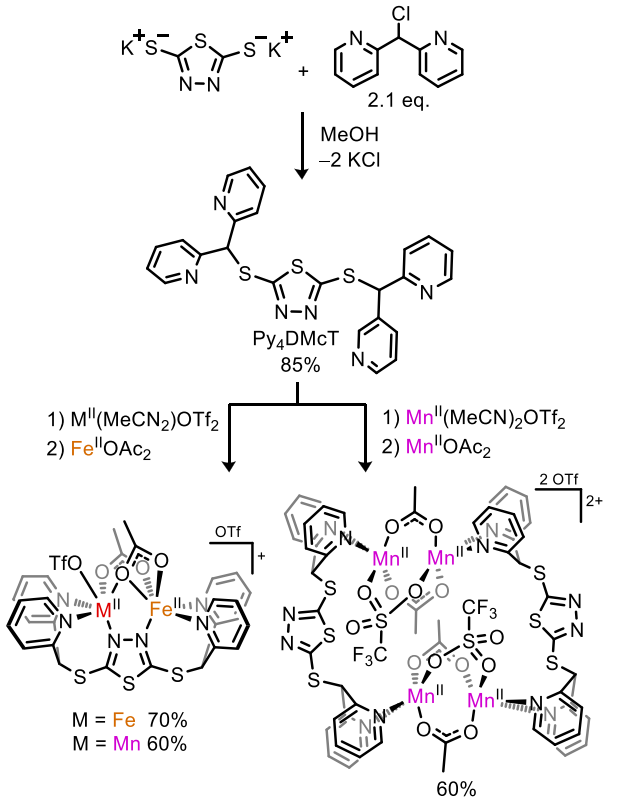


**Scheme 2. Symmetric versus Unsymmetric Acetate Binding Modes**

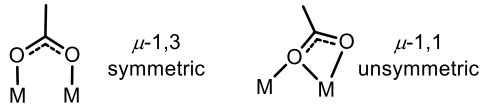


compared to the 3.46409(16) Å distance in $\mathbf{Fe^{II}Fe^{II}}$, consistent with the larger atomic radius of $Mn^{II}$ versus $Fe^{II}$.

While an unsymmetric $\mu$-1,1 carboxylate ligand (Scheme 2) is a common structural feature in RNRs, R2lox, and BMMs,[31−34] it is not as common in synthetic systems.[52−57] Notably, a $\mu$-1,1 carboxylate ligand has never been reported in a synthetic Mn/Fe complex until now. In our synthetic system, the unsymmetric acetate replicates the unsymmetric carboxylates in RNRIc (E227) and R2lox (E202), producing the same site-specific geometries as the enzymes. The unsymmetric $\mu$-1,1 binding of acetate in $\mathbf{Fe^{II}Fe^{II}}$ and $\mathbf{Mn^{II}Fe^{II}}$ is likely promoted by the outward tilting of the metal $z$-axes following coordination of the metal centers to the N atoms of the thiadiazole ring. Similar outward tilting of the metal $z$-axes can be observed in RNRIc and R2lox (see the Supporting Information, Figure S36), although such a structural feature is not unique to these enzymes.[31−34,58] In our complexes, the N atoms of the central ring form a template for a short M−M distance, making the six-membered metallacycle of $\mu$-1,1/$\mu$-1,3 binding mode more favorable than the eight-membered metallacycle of $\mu$-1,3/$\mu$-1,3 binding mode.

The overall structure of $\mathbf{Mn^{II}Fe^{II}}$ more closely resembles the unsymmetric core of R2lox, as it lacks the solvent-derived O-atom bridge present in RNRIc. Further, the metal separation in $\mathbf{Mn^{II}Fe^{II}}$ is more comparable to the M−M distance seen in R2lox (3.65 Å)[19] than RNRIc (3.2 Å).[25] Given the structural

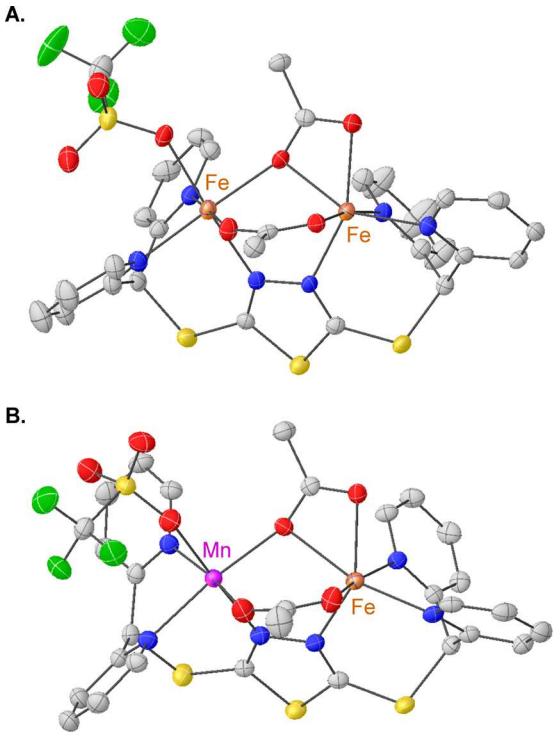


**Figure 3.** Solid-state structures of (A) $\mathbf{Fe^{II}Fe^{II}}$ and (B) $\mathbf{Mn^{II}Fe^{II}}$ with thermal ellipsoids shown at 50% level of probability. The outer sphere triflate counter anion and co-crystallized dichloromethane solvent molecules are omitted for clarity.

similarities between $\mathbf{Mn^{II}Fe^{II}}$ and R2lox, we tentatively assigned the metal center at the distorted octahedral site as $Fe^{II}$. Such an assignment also results in a better agreement with the electron density map, where $R_1$ = 4.30% vs 4.46% with a reversed Fe/Mn assignment.

The heterobimetallic identity of $\mathbf{Mn^{II}Fe^{II}}$ was further confirmed by spectroscopic analysis. The $^1$H NMR spectrum of $\mathbf{Mn^{II}Fe^{II}}$ reveals eight broad resonances from −30 to 140 ppm that are distinct from the paramagnetic peaks of $\mathbf{Fe^{II}Fe^{II}}$ (Figure 4A), consistent with the unsymmetric nature of $\mathbf{Mn^{II}Fe^{II}}$.[39] Mössbauer spectroscopy reveals that $\mathbf{Fe^{II}Fe^{II}}$ is best fitted with two distinct iron sites, whereas $\mathbf{Mn^{II}Fe^{II}}$ is fitted best with a single iron site (Figure 4B,C). The isomer shifts of $\mathbf{Fe^{II}Fe^{II}}$ ($\delta_1$ = 1.20 mm s$^{-1}$, $\delta_2$ = 1.22 mm s$^{-1}$) and $\mathbf{Mn^{II}Fe^{II}}$ ($\delta$ = 1.28 mm s$^{-1}$) are consistent with high-spin $Fe^{II}$ centers and are similar to the reported value for the $Mn^{II}Fe^{II}$ cofactor of R2lox ($\delta$ = 1.28 mm s$^{-1}$).[20] This indicates that $\mathbf{Mn^{II}Fe^{II}}$ accurately models not only the geometry of the heterobimetallic cofactor but also the spin state of the metal ions. X-band electron paramagnetic resonance spectroscopy (EPR) of $\mathbf{Mn^{II}Fe^{II}}$ shows a broad S = 1/2 signal (Figure S7), similar to the EPR spectra of $Mn^{II}Fe^{II}$ complexes reported by Que et al. and Carboni et al.[44,48] Inductively coupled plasma mass spectrometry (ICP-MS) analysis of $\mathbf{Mn^{II}Fe^{II}}$ indicates the incorporation of $Fe^{II}$ and $Mn^{II}$ in approximately a 1:1 ratio (4.16% $Fe^{II}$ to 4.74% $Mn^{II}$).

After the isolation and characterization of $\mathbf{Fe^{II}Fe^{II}}$ and $\mathbf{Mn^{II}Fe^{II}}$, we attempted to complete the series of bimetallic complexes by preparing the analogous dimanganese species. However, treatment of **L** with $Mn^{II}(OAc)_2$ and $Mn(OTf)_2MeCN_2$ resulted in the isolation of a colorless, NMR-silent tetramanganese paddlewheel complex, $\mathbf{Mn^{II}_4}$ (Scheme 2, right).[39,59] Single-crystal XRD analysis shows two dimanganese



https://doi.org/10.1021/jacs.2c11930
J. Am. Chem. Soc. 2023, 145, 3491−3498

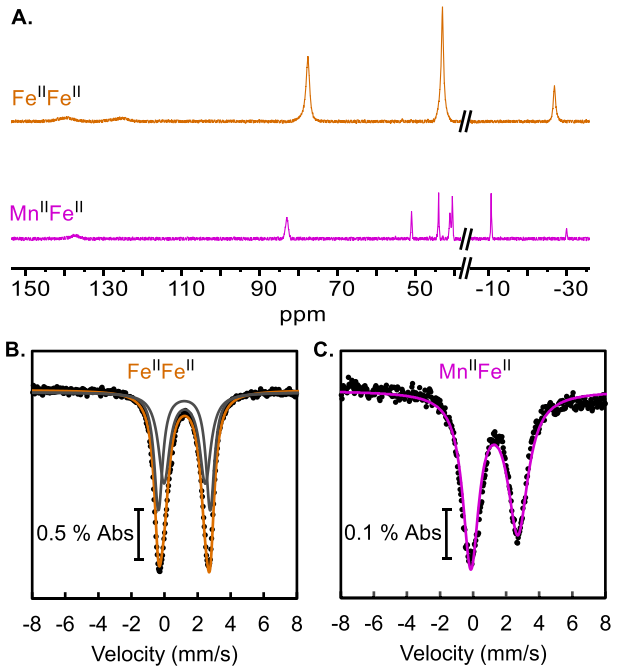


**Figure 4.** (A) $^1$H NMR spectra of $\mathbf{Fe^{II}Fe^{II}}$ (orange) and $\mathbf{Mn^{II}Fe^{II}}$ (pink), 2.5 mM in $CD_2Cl_2$. Solid-state $^{57}$Fe Mössbauer spectra of (B) $\mathbf{Fe^{II}Fe^{II}}$ and (C) $\mathbf{Mn^{II}Fe^{II}}$.

paddlewheels sandwiched between two $Py_4DMcT$ ligands, with all $Mn^{II}$ ions symmetrically bridged by two acetate anions and one triflate anion, and a Mn−Mn distance of 3.860 Å (see the SI, Figure S35). The formation of the tetramanganese complex, rather than a dimanganese species, suggests that **L** is unable to accommodate two $Mn^{II}$ centers in the same bimetallic environment, perhaps due to the larger size of $Mn^{II}$ versus $Fe^{II}$. This observation also coincides with the lack of $Mn^{II}Mn^{II}$ cofactor formation in R2lox.[16,19,20,23,24]

**Heterobimetallic Selectivity.** With the spectroscopic characterization of $\mathbf{Fe^{II}Fe^{II}}$, $\mathbf{Mn^{II}Fe^{II}}$, and $\mathbf{Mn^{II}_4}$, we wanted to determine whether **L** could reproduce RNRIc and R2lox's ability to selectively assemble a heterobimetallic Mn/Fe center. Importantly, $\mathbf{Mn^{II}Fe^{II}}$ is stable in $CD_2Cl_2$ at room temperature without noticeable metal scrambling for at least 12 h (Figure S8), allowing the use of in situ $^1$H NMR to quantify $\mathbf{Mn^{II}Fe^{II}}$ formation. First, we investigated whether the order of addition of $Fe^{II}$ and $Mn^{II}$ sources to **L** influences the yield of $\mathbf{Mn^{II}Fe^{II}}$. Ligand **L** was treated with $Fe^{II}$ and $Mn^{II}$ sources in different orders. Regardless of the order of addition, the resulting $^1$H NMR spectra show that $\mathbf{Mn^{II}Fe^{II}}$ is produced in similar yields (74−77%; Table 1) with minimal (ca. 6%) $\mathbf{Fe^{II}Fe^{II}}$ contamination. As $\mathbf{Mn^{II}Fe^{II}}$ is the major product under all conditions, we posited that the formation of $\mathbf{Mn^{II}Fe^{II}}$ likely occurs selectively via the same assembly route, no matter the order of metal addition. Indeed, treatment of **L** with a mixture of one equivalent each of $Fe^{II}$ and $Mn^{II}$ sources simultaneously affords $\mathbf{Mn^{II}Fe^{II}}$ in 80% yield with 8% $\mathbf{Fe^{II}Fe^{II}}$ contamination (Table 2). Our attempts to characterize a monometallic state (**L**:M = 1:1) en route to $\mathbf{Mn^{II}Fe^{II}}$ were unsuccessful. Addition of one equivalent of $M^{II}$ to **L** in the presence of acetate leads to the formation of the bimetallic complex as the major product (see the SI, Figures S34 and S35). When acetate is not present in the reaction mixture, the combination of $M^{II}$ and **L** in a 1:1 ratio results in an intractable mixture of products.

**Table 1. $^1$H NMR Yields of $\mathbf{Fe^{II}Fe^{II}}$ and $\mathbf{Mn^{II}Fe^{II}}$ under Various Metalation Conditions**

| order of addition of metal salts | yield of $\mathbf{Fe^{II}Fe^{II}}$ | yield of $\mathbf{Mn^{II}Fe^{II}}$ |
|---|---|---|
| (1) $Fe^{II}(OTf)_2MeCN_2$ (2) $Mn^{II}(OAc)_2$ | 6.6% | 77.0% |
| (1) $Mn^{II}(OTf)_2MeCN_2$ (2) $Fe^{II}(OAc)_2$ | 5.8% | 75.4% |
| (1) $Fe^{II}(OAc)_2$ (2) $Mn^{II}(OTf)_2MeCN_2$ | 5.8% | 73.8% |
| (1) $Mn^{II}(OAc)_2$ (2) $Fe^{II}(OTf)_2MeCN_2$ | 6.6% | 77.0% |

**Table 2. $^1$H NMR Yields of $\mathbf{Mn^{II}Fe^{II}}$ as a Function of the Ratio of $Fe^{II}$:$Mn^{II}$:L**

| $Fe^{II}$:$Mn^{II}$:L/Apo-protein | % $\mathbf{Fe^{II}Fe^{II}}$ | % $\mathbf{Mn^{II}Fe^{II}}$ | ref |
|---|---|---|---|
| 1:1:1 **L** | 8.0% | 80.0% | this work |
| 1.25:1.25:1 **L** | 9.0% | 75.0% | this work |
| 1.50:1.50:1 **L** | 20.0% | 72.0% | this work |
| 1.75:1.75:1 **L** | 41.0% | 49.0% | this work |
| 2:2:1 **L** | 61.0% | 0% | this work |
| 2:2:1 R2lox | 61% | 21% | ref 20 |

We further investigated the influence of "metal availability" on heterobimetallic selectivity. The ligand **L** was subjected to a series of reactions with increasing amounts of equimolar Fe and Mn sources. In all reactions, $Fe^{II}(OTf)_2MeCN_2$ and $Mn^{II}(OTf)_2MeCN_2$ were premixed before being added to one equivalent of **L**. The reaction was allowed to stir for several minutes before acetate was added in the form of TBAOAc. The resulting solution was then analyzed by $^1$H NMR spectroscopy (Table 2).

Strikingly, as the metal availability increased from one equivalent to two equivalents of $Fe^{II}/Mn^{II}$ per **L**, the yield of $\mathbf{Mn^{II}Fe^{II}}$ decreases, and the yield of $\mathbf{Fe^{II}Fe^{II}}$ increases. When two equivalents of $Fe^{II}$ and $Mn^{II}$ ions are available, no $\mathbf{Mn^{II}Fe^{II}}$ formation is observed, implying that the formation of the heterobimetallic species is only favored under $Fe^{II}$-deficient conditions. With two equivalents of $Fe^{II}/Mn^{II}$ per **L**, the binding of $Fe^{II}$ outcompetes that of $Mn^{II}$ completely, which is in agreement with the higher binding affinity of $Fe^{II}$ over $Mn^{II}$, as predicted by the classical Irving−Williams series.[30] The availability of $Mn^{II}$ vs $Fe^{II}$ in biological environments has been invoked as a potential reason for why the heterobimetallic Mn/Fe cofactors form.[3−5,11]

While there is not a complete reversal in selectivity of the RNRIc and R2lox cofactors under Fe-rich conditions, higher $Fe^{II}$ concentrations have also been found to inhibit heterobimetallic cofactor assembly.[20] Thus, the increased yield of $\mathbf{Fe^{II}Fe^{II}}$ in our system under Fe-rich conditions is similar to that observed for R2lox and RNRIc.[18−20] The stronger binding affinity of $Fe^{II}$ versus $Mn^{II}$ is further supported by a computational study.[19] The relative stabilities of each $\mathbf{M^{II}M^{II}}$ complex (M = Fe or Mn) were determined by comparing the energy sum of the bimetallic complex with different combinations of solvated metal ions (Table 3).[19] Broken-symmetry density functional theory (DFT) calculations at the B3LYP/def2-TZVP level of theory show that the formation of $\mathbf{Fe^{II}Fe^{II}}$ is more favorable than $\mathbf{Mn^{II}Fe^{II}}$ by 4.6 kcal/mol. The $\mathbf{Fe^{II}Mn^{II}}$ complex with a reversed metal occupancy and the theoretical $\mathbf{Mn^{II}Mn^{II}}$ species are less stable than $\mathbf{Mn^{II}Fe^{II}}$ by 2.5 and 5.6 kcal/mol, respectively. These results follow the same trend as an analogous study performed on the R2lox cofactor.[19]


https://doi.org/10.1021/jacs.2c11930
J. Am. Chem. Soc. 2023, 145, 3491−3498

Table 3. DFT-Computed Relative Energies (B3LYP/def2-TZVP) for the Binding of Different Combinations of $Fe^{II}$ and $Mn^{II}$ to L

| bimetallic complex | solvated ions | relative energy (kcal/mol) |
|---|---|---|
| $Fe^{II}Fe^{II}$ | $Mn^{II}$, $Mn^{II}$ | 0.0 |
| $Mn^{II}Fe^{II}$ (Fe at distorted site) | $Mn^{II}$, $Fe^{II}$ | +4.6 |
| $Fe^{II}Mn^{II}$ (Mn at distorted site) | $Fe^{II}$, $Mn^{II}$ | +7.1 |
| $Mn^{II}Mn^{II}$ | $Fe^{II}$, $Fe^{II}$ | +10.2 |

**Anomalous XRD Study.** In addition to the bioavailability of $Fe^{II}$, the inequivalent metal binding sites in R2lox (distorted versus octahedral site) have also been regarded as a potential influence on the selective formation of the heterobimetallic cofactor. As $Mn^{II}Fe^{II}$ contains structurally analogous differentiated metal binding sites and exhibits similar selective assembly to R2lox and RNRIc, we wanted to further understand site selectivity in $Mn^{II}Fe^{II}$ via single-crystal anomalous XRD.

Anomalous XRD allows for a quantitative determination of the amount of metal present at a particular crystallographic site.[38,60,61] Unlike traditional XRD, metal centers with similar numbers of electrons can be differentiated by exploiting the differences in their K-edge absorption energies.[62] At a synchrotron source, we collected several anomalous data sets at 50 eV above and below the $Fe^{II}$ and $Mn^{II}$ absorption edges. Additionally, a data set was collected at 30 keV, far from the absorption edges of any atoms. As the incident X-ray wavelength approaches the K-edge energy of a metal, the anomalous scattering terms ($f'$, $f''$) of the atomic scattering factor ($f$, where $f(\lambda) = f^0 + f' + if''$) become more pronounced (Figure 5A). Under these conditions, $f'$ and $f''$ can be utilized to quantify the amount of metal present at each site (Figure 5B and Table 4).[38,60,61] Gratifyingly, we observed primary occupation of $Fe^{II}$ at the distorted site (82.0%) and primary occupation of $Mn^{II}$ at the octahedral site (73.0%).

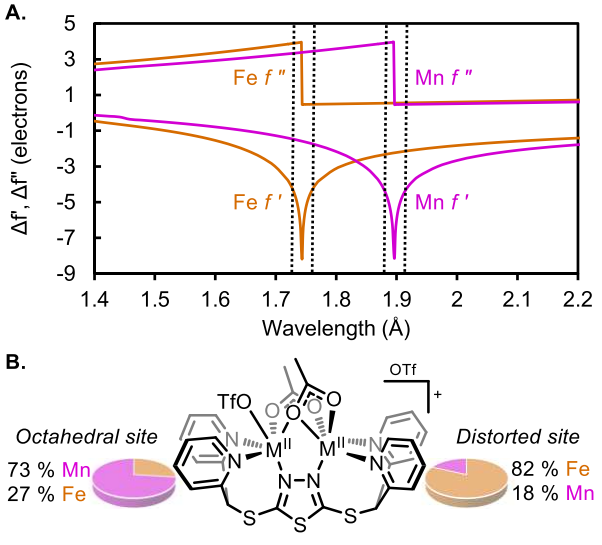


Figure 5. (A) Theoretical anomalous dispersion corrections with the real ($\Delta f'$) and imaginary ($\Delta f''$) scattering factors for Fe (orange) and Mn (pink) as functions of wavelength. Anomalous data were collected at the wavelengths highlighted with dashed lines. (B) Metal occupancies determined based on experimental $f'$ values of four sets of anomalous XRD data.

Table 4. Results of Single-Crystal Anomalous XRD Studies for $Mn^{II}Fe^{II}$, R2lox, and RNRIc

| | distorted site | | octahedral site | | |
|---|---|---|---|---|---|
| | % Fe | % Mn | % Fe | % Mn | ref |
| $Mn^{II}Fe^{II}$[a] | 82% | 18% | 27% | 73% | this work |
| RNRIc[b] | 100% | 0% | 0% | 100% | ref 6 |
| R2lox[c] | 80% | 21% | 48% | 53% | ref 19 |
| R2lox[d] | 69% | 31% | 18% | 82% | ref 19 |
| R2lox[e] | 92% | 8% | 20% | 80% | ref 20 |

[a]Single crystals isolated from a solution with 1:1 $Fe^{II}$ and $Mn^{II}$ under an $N_2$ atmosphere. Average of two data sets. [b]Protein crystals isolated after sequential metal loading in the presence of $O_2$. [c]Apo-R2lox crystals soaked for 1 h in excess, equal concentrations of $Mn^{II}/Fe^{II}$ in the absence of $O_2$. Average of two data sets. [d]Apo-R2lox crystals soaked for 1 h in excess, equal concentrations of $Mn^{II}/Fe^{II}$ in the presence of $O_2$. Average of two data sets. [e]Recrystallization of R2lox after reconstitution in a 2:1 ratio of $Mn^{II}/Fe^{II}$ in the presence of $O_2$. Average of two data sets.

Interestingly, the selectivity of the distorted and octahedral sites by $Mn^{II}Fe^{II}$ is quite similar to RNRIc and R2lox (Table 4). Both R2lox and RNRIc display a preference for $Fe^{II}$ coordination at the distorted site and $Mn^{II}$ coordination at the octahedral site (Table 4).[6,19,20] It was proposed that the facile activation of $O_2$ at the correctly assembled $Mn^{II}Fe^{II}$ site enriches MnFe cofactors. Exposure to oxygen represents an irreversible step in the maturation process, in which the metals are "locked in place" as the less labile $Mn^{III}Fe^{III}$ cofactors.[16] Our study suggests that selective formation of the MnFe site can also be accomplished in high accuracy at the reduced state (II,II).

## DISCUSSION

The simplicity of our synthetic system allows us to draw several conclusions regarding the mechanism of $Mn^{II}Fe^{II}$ formation (Scheme 3A). We successfully determined that the binding of $Fe^{II}$ is favored as both the first and the second metal, as the yield of $Mn^{II}Fe^{II}$ is reduced to 0% when two equivalents of $Fe^{II}$ are present. Under conditions where only one equivalent of each metal is present per **L**, the more favorable binding of $Fe^{II}$ to **L** results in a $Mn^{II}$-rich environment, which promotes the loading of $Mn^{II}$ as the second metal (Scheme 3A). Since the binding of $Fe^{II}$ outcompetes that of $Mn^{II}$ (in accordance with the Irving–Williams series), the formation of $Mn^{II}Fe^{II}$ must result from the depletion of $Fe^{II}$ in the solution. $Fe^{II}$ depletion can be attributed to two potential reasons: (1) highly selective binding of $Fe^{II}$ as the first metal and (2) the inability of **L** to coordinate two $Mn^{II}$ ions. Even if the first binding step is not perfectly selective for $Fe^{II}$, the monometallic $LMn^{II}$ cannot bind another $Mn^{II}$ ion to form a bimetallic $Mn^{II}Mn^{II}$ complex, preventing further consumption of $Mn^{II}$ ions in the solution (Scheme 3A).

The proposed mechanism of assembly of $Mn^{II}Fe^{II}$ more closely resembles that of R2lox, where the formation of the Mn/Fe cofactor occurs via initial coordination of $Fe^{II}$, followed by $Mn^{II}$ (Scheme 3B). Rather than loading $Mn^{II}$ and $Fe^{II}$ in a stepwise fashion, apo-RNRIc first loads two $Mn^{II}$ ions and then preferentially substitutes one $Mn^{II}$ for $Fe^{II}$ at the distorted site (Scheme 3C). A difference between our synthetic system and RNRIc and R2lox is that the natural proteins have either one (R2lox) or two (RNRIc) pre-organized metal binding sites, whereas the metal binding sites in our system are only


https://doi.org/10.1021/jacs.2c11930
J. Am. Chem. Soc. 2023, 145, 3491−3498

**Scheme 3. Assembly of Synthetic Complex versus Enzyme Cofactors**

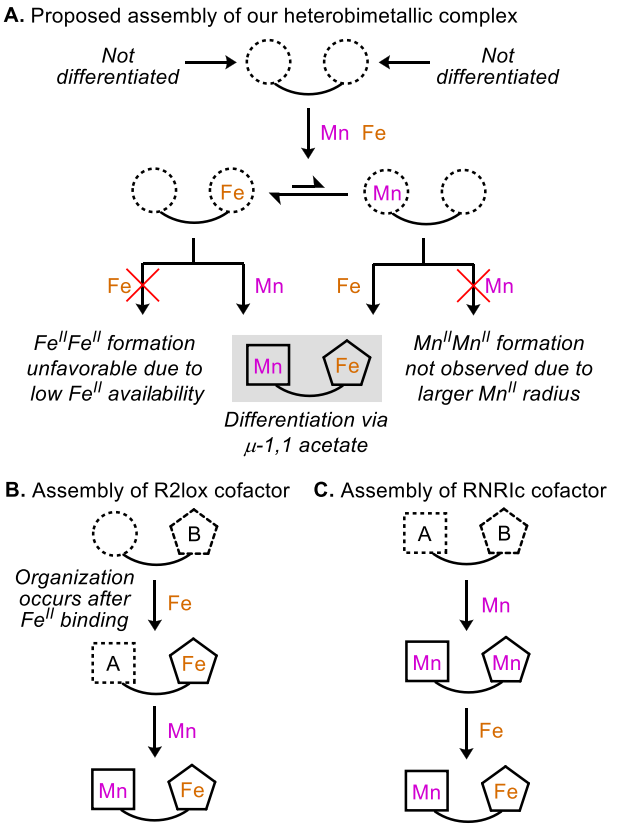


differentiated upon acetate binding. Nonetheless, the end result, following acetate coordination, is the same site-differentiated Mn/Fe species, with $Mn^{II}$ occupying the octahedral site and $Fe^{II}$ occupying the distorted site, suggesting that the unsymmetric carboxylate is an essential structural feature for correct site selectivity ($Mn^{II}$ in octahedral site and $Fe^{II}$ in distorted site). More importantly, however, metal availability (an iron deficiency) is the first key requirement that allows for Mn/Fe cofactor formation. The importance of metal availability is emphasized by the decreased yields of synthetic and enzymatic heterobimetallic species in the presence of excess Fe.

## CONCLUSIONS

In summary, we have reported a series of synthetic model complexes, **$Fe^{II}Fe^{II}$**, **$Mn^{II}Fe^{II}$**, and **$Mn^{II}_4$**, which have shed light onto the mechanism of heterobimetallic assembly in R2lox and RNRIc. While **L** was not able to accommodate a dimanganese complex in the solid state, single-crystal X-ray analysis of **$Fe^{II}Fe^{II}$** and **$Mn^{II}Fe^{II}$** displayed a bimetallic core containing an unsymmetrically bridged carboxylate ligand. The carboxylate differentiates the metal binding sites and results in a heterobimetallic complex that models the binding of $Fe^{II}$ and $Mn^{II}$ observed in RNRIc and R2lox, i.e., $Fe^{II}$ coordination at the distorted site and $Mn^{II}$ coordination at the octahedral site, which was confirmed via anomalous XRD.

Our model study provides an alternative explanation as to why R2lox and RNRIc appear to be violating the fundamental thermodynamic rules governing coordination chemistry. The favorable binding of $Fe^{II}$ over $Mn^{II}$ along with a site-differentiating $\mu$-1,1-carboxylate was sufficient for correct heterobimetallic assembly. Despite the overall results of the reaction appearing to be contrary to the binding affinities of $Fe^{II}$ versus $Mn^{II}$, the Irving–Williams series was not being circumvented. The $\mu$-1,1-carboxylate is a feature shared by both R2lox and RNRIc in the reduced state, as is the observation of favorable diiron cofactor formation under increased concentrations of iron. Therefore, metal availability and site differentiation are two of the most critical factors to correct cofactor assembly in RNRIc and R2lox. This hypothesis is also consistent with the observation that the intracellular availability of metal ions plays a role in metal selection.[4,5,19] Beyond correct cofactor formation, we believe that site differentiation likely has implications toward oxidative reactivity, as observed in R2lox.[16] These intriguing questions will be the subject of our future studies.

## ASSOCIATED CONTENT

### Supporting Information

The Supporting Information is available free of charge at https://pubs.acs.org/doi/10.1021/jacs.2c11930.

Experimental details, including characterization data, spectra, computational procedures, and results, and crystallographic data for $[Fe^{II}_2Py_4DMcT(OAc)_2(OTf)][OTf]$ (CSD: 2218376), $[Mn^{II}Fe^{II}Py_4DMcT(OAc)_2(OTf)][OTf]$ (CSD: 2218377), and $[Mn^{II}_4(Py_4DMcT)_2(OAc)_4(OTf)_2][OTf]_2$ (CSD: 2218378) (PDF)

### Accession Codes

CCDC 2218376–2218378 contain the supplementary crystallographic data for this paper. These data can be obtained free of charge via www.ccdc.cam.ac.uk/data_request/cif, or by emailing data_request@ccdc.cam.ac.uk, or by contacting The Cambridge Crystallographic Data Centre, 12 Union Road, Cambridge CB2 1EZ, UK; fax: +44 1223 336033.

## AUTHOR INFORMATION


### Corresponding Author

**Shiyu Zhang** – *Department of Chemistry & Biochemistry, The Ohio State University, Columbus, Ohio 43210, United States*; orcid.org/0000-0002-2536-4324; Email: zhang.8941@osu.edu

### Authors

**Anna L. Poptic** – *Department of Chemistry & Biochemistry, The Ohio State University, Columbus, Ohio 43210, United States*

**Ying-Pin Chen** – *ChemMatCARS, University of Chicago, Argonne, Illinois 60439, United States*

**Tieyan Chang** – *ChemMatCARS, University of Chicago, Argonne, Illinois 60439, United States*

**Yu-Sheng Chen** – *ChemMatCARS, University of Chicago, Argonne, Illinois 60439, United States*

**Curtis E. Moore** – *Department of Chemistry & Biochemistry, The Ohio State University, Columbus, Ohio 43210, United States*; orcid.org/0000-0002-3311-7155

Complete contact information is available at: https://pubs.acs.org/10.1021/jacs.2c11930


### Notes

The authors declare no competing financial interest.



https://doi.org/10.1021/jacs.2c11930
J. Am. Chem. Soc. 2023, 145, 3491–3498

## ■ ACKNOWLEDGMENTS

A.L.P. would like to extend her thanks to Dr. Dan Conroy and Dr. Curtis Moore for their help with NMR spectroscopy and single-crystal XRD. We would also like to thank Prof. Hannah Shafaat for her valuable insights and discussions. This publication is based on work funded partially by a Pelotonia Graduate Fellowship awarded to A.L.P. and by the National Science Foundation under award no. CHE-1904560. The authors acknowledge the Ohio Supercomputer Center for high-performance computing resources and The Ohio State University Department of Chemistry and Biochemistry for additional financial support and resources. ChemMatCARS Sector 15 is supported by the National Science Foundation under grant number NSF/CHE-1834750. This research used resources of the Advanced Photon Source, a U.S. Department of Energy (DOE) Office of Science User Facility operated for the DOE Office of Science by Argonne National Laboratory under contract no. DE-AC02-06CH11357.

## ■ REFERENCES

(1) Mitić, N.; Smith, S. J.; Neves, A.; Guddat, L. W.; Gahan, L. R.; Schenk, G. The Catalytic Mechanisms of Binuclear Metallohydrolases. *Chem. Rev.* **2006**, *106*, 3338−3363.
(2) Nordlund, P.; Reichard, P. Ribonucleotide Reductases. *Annu. Rev. Biochem.* **2006**, *75*, 681−706.
(3) Cotruvo, J. A., Jr.; Stubbe, J. Class I Ribonucleotide Reductases: Metallocofactor Assembly and Repair In Vitro and In Vivo. *Annu. Rev. Biochem.* **2011**, *80*, 733−767.
(4) Cotruvo, J. A., Jr.; Stubbe, J. Metallation and Mismetallation of Iron and Manganese Proteins in Vitro and in Vivo: The Class I Ribonucleotide Reductases as a Case Study. *Metallomics* **2012**, *4*, 1020−1036.
(5) Huang, M.; Parker, M. J.; Stubbe, J. Choosing the Right Metal: Case Studies of Class I Ribonucleotide Reductases. *J. Biol. Chem.* **2014**, *289*, 28104−28111.
(6) Dassama, L. M. K.; Krebs, C.; Bollinger, J. M., Jr.; Rosenzweig, A. C.; Boal, A. K. Structural Basis for Assembly of the $Mn^{IV}/Fe^{III}$ Cofactor in the Class Ic Ribonucleotide Reductase from Chlamydia Trachomatis. *Biochemistry* **2013**, *52*, 6424−6436.
(7) Jiang, W.; Yun, D.; Saleh, L.; Barr, E. W.; Xing, G.; Hoffart, L. M.; Maslak, M. A.; Krebs, C.; Bollinger, J. M. A Manganese(IV)/Iron(III) Cofactor in Chlamydia Trachomatis Ribonucleotide Reductase. *Science* **2007**, *316*, 1188−1191.
(8) Jiang, W.; Hoffart, L. M.; Krebs, C.; Bollinger, J. M. A Manganese(IV)/Iron(IV) Intermediate in Assembly of the Manganese(IV)/Iron(III) Cofactor of Chlamydia Trachomatis Ribonucleotide Reductase†. *Biochemistry* **2007**, *46*, 8709−8716.
(9) Jiang, W.; Yun, D.; Saleh, L.; Bollinger, J. M., Jr.; Krebs, C. Formation and Function of the Manganese(IV)/Iron(III) Cofactor in Chlamydia Trachomatis Ribonucleotide Reductase. *Biochemistry* **2008**, *47*, 13736−13744.
(10) Högbom, M. The Manganese/Iron-Carboxylate Proteins: What Is What, Where Are They, and What Can the Sequences Tell Us? *J. Biol. Inorg. Chem.* **2010**, *15*, 339−349.
(11) Högbom, M. Metal Use in Ribonucleotide Reductase R2, Di-Iron, Di-Manganese and Heterodinuclear—an Intricate Bioinorganic Workaround to Use Different Metals for the Same Reaction. *Metallomics* **2011**, *3*, 110−120.
(12) Griese, J. J.; Kositzki, R.; Haumann, M.; Högbom, M. Assembly of a Heterodinuclear Mn/Fe Cofactor Is Coupled to Tyrosine−Valine Ether Cross-Link Formation in the R2-like Ligand-Binding Oxidase. *J. Biol. Inorg. Chem.* **2019**, *24*, 211−221.
(13) Diamanti, R.; Srinivas, V.; Johansson, A. I.; Nordström, A.; Griese, J. J.; Lebrette, H.; Högbom, M. Comparative Structural Analysis Provides New Insights into the Function of R2-like Ligand-Binding Oxidase. *FEBS Lett.* **2022**, *596*, 1600−1610.
(14) Miller, E. K.; Trivelas, N. E.; Maugeri, P. T.; Blaesi, E. J.; Shafaat, H. S. Time-Resolved Investigations of Heterobimetallic Cofactor Assembly in R2lox Reveal Distinct Mn/Fe Intermediates. *Biochemistry* **2017**, *56*, 3369−3379.
(15) Maugeri, P. T.; Griese, J. J.; Branca, R. M.; Miller, E. K.; Smith, Z. R.; Eirich, J.; Högbom, M.; Shafaat, H. S. Driving Protein Conformational Changes with Light: Photoinduced Structural Rearrangement in a Heterobimetallic Oxidase. *J. Am. Chem. Soc.* **2018**, *140*, 1471−1480.
(16) Kisgeropoulos, E. C.; Griese, J. J.; Smith, Z. R.; Branca, R. M. M.; Schneider, C. R.; Högbom, M.; Shafaat, H. S. Key Structural Motifs Balance Metal Binding and Oxidative Reactivity in a Heterobimetallic Mn/Fe Protein. *J. Am. Chem. Soc.* **2020**, *142*, 5338−5354.
(17) Kisgeropoulos, E. C.; Gan, Y. J.; Greer, S. M.; Hazel, J. M.; Shafaat, H. S. Pulsed Multifrequency Electron Paramagnetic Resonance Spectroscopy Reveals Key Branch Points for One- vs Two-Electron Reactivity in Mn/Fe Proteins. *J. Am. Chem. Soc.* **2022**, *144*, 11991−12006.
(18) Griese, J. J.; Srinivas, V.; Högbom, M. Assembly of Nonheme Mn/Fe Active Sites in Heterodinuclear Metalloproteins. *J. Biol. Inorg. Chem.* **2014**, *19*, 759−774.
(19) Griese, J. J.; Roos, K.; Cox, N.; Shafaat, H. S.; Branca, R. M. M.; Lehtiö, J.; Gräslund, A.; Lubitz, W.; Siegbahn, P. E. M.; Högbom, M. Direct Observation of Structurally Encoded Metal Discrimination and Ether Bond Formation in a Heterodinuclear Metalloprotein. *Proc. Natl. Acad. Sci. U. S. A.* **2013**, *110*, 17189−17194.
(20) Kutin, Y.; Srinivas, V.; Fritz, M.; Kositzki, R.; Shafaat, H. S.; Birrell, J.; Bill, E.; Haumann, M.; Lubitz, W.; Högbom, M.; Griese, J. J.; Cox, N. Divergent Assembly Mechanisms of the Manganese/Iron Cofactors in R2lox and R2c Proteins. *J. Inorg. Biochem.* **2016**, *162*, 164−177.
(21) Högbom, M.; Stenmark, P.; Voevodskaya, N.; McClarty, G.; Gräslund, A.; Nordlund, P. The Radical Site in Chlamydial Ribonucleotide Reductase Defines a New R2 Subclass. *Science* **2004**, *305*, 245−248.
(22) Andersson, C. S.; Högbom, M. A Mycobacterium Tuberculosis Ligand-Binding Mn/Fe Protein Reveals a New Cofactor in a Remodeled R2-Protein Scaffold. *Proc. Natl. Acad. Sci. U. S. A.* **2009**, *106*, 5633−5638.
(23) Shafaat, H. S.; Griese, J. J.; Pantazis, D. A.; Roos, K.; Andersson, C. S.; Popović-Bijelić, A.; Gräslund, A.; Siegbahn, P. E. M.; Neese, F.; Lubitz, W.; Högbom, M.; Cox, N. Electronic Structural Flexibility of Heterobimetallic Mn/Fe Cofactors: R2lox and R2c Proteins. *J. Am. Chem. Soc.* **2014**, *136*, 13399−13409.
(24) Griese, J. J.; Kositzki, R.; Schrapers, P.; Branca, R. M. M.; Nordström, X. A.; Lehtiö, J.; Haumann, M.; Högbom, X. M. Structural Basis for Oxygen Activation at a Heterodinuclear Manganese/Iron Cofactor. *J. Biol. Chem.* **2015**, *290*, 25254−25272.
(25) Kutin, Y.; Kositzki, R.; Branca, R. M. M.; Srinivas, V.; Lundin, D.; Haumann, M.; Högbom, M.; Cox, N.; Griese, J. J. Chemical Flexibility of Heterobimetallic Mn/Fe Cofactors: R2lox and R2c Proteins. *J. Biol. Chem.* **2019**, *294*, 18372−18386.
(26) Manley, O. M.; Phan, H. N.; Stewart, A. K.; Mosley, D. A.; Xue, S.; Cha, L.; Bai, H.; Lightfoot, V. C.; Rucker, P. A.; Collins, L.; Williams, T. I.; Chang, W. C.; Guo, Y.; Makris, T. M. Self-Sacrificial Tyrosine Cleavage by an Fe:Mn Oxygenase for the Biosynthesis of Para-Aminobenzoate in Chlamydia Trachomatis. *Proc. Natl. Acad. Sci. U. S. A.* **2022**, *119*, 1−7.
(27) Waldron, K. J.; Rutherford, J. C.; Ford, D.; Robinson, N. J. Metalloproteins and Metal Sensing. *Nature* **2009**, *460*, 823−830.
(28) Smethurst, D. G. J. J.; Shcherbik, N. Interchangeable Utilization of Metals: New Perspectives on the Impacts of Metal Ions Employed in Ancient and Extant Biomolecules. *J. Biol. Chem.* **2021**, *297*, 1−23.
(29) Choi, T. S.; Tezcan, F. A. Overcoming Universal Restrictions on Metal Selectivity by Protein Design. *Nature* **2022**, *603*, 522−527.
(30) Irving, H.; Williams, R. J. P. The Stability of Transition-Metal Complexes. *J. Chem. Soc.* **1953**, 3192−3210.


https://doi.org/10.1021/jacs.2c11930
J. Am. Chem. Soc. 2023, 145, 3491−3498

(31) Rosenzweig, A. C.; Frederick, C. A.; Lippard, S. J.; Nordlund, P. Crystal Structure of a Bacterial Non-Haem Iron Hydroxylase That Catalyses the Biological Oxidation of Methane. *Nature* **1993**, *366*, 537−543.
(32) Rosenzweig, A. C.; Lippard, S. J. Determining the Structure of a Hydroxylase Enzyme That Catalyzes the Conversion of Methane to Methanol in Methanotrophic Bacteria. *Acc. Chem. Res.* **1994**, *27*, 229−236.
(33) Rosenzweig, A. C.; Nordlund, P.; Takahara, P. M.; Frederick, C. A.; Lippard, S. J. Geometry of the Soluble Methane Monooxygenase Catalytic Diiron Center in Two Oxidation States. *Chem. Biol.* **1995**, *2*, 409−418.
(34) Whittington, D. A.; Lippard, S. J. Crystal Structures of the Soluble Methane Monooxygenase Hydroxylase from Methylococcus Capsulatus (Bath) Demonstrating Geometrical Variability at the Dinuclear Iron Active Site. *J. Am. Chem. Soc.* **2001**, *123*, 827−838.
(35) Borovik, A. S.; Que, L.; Papaefthymiou, V.; Muenck, E.; Taylor, L. F.; Anderson, O. P. Heterobimetallic Complexes with (μ-Phenoxo)Bis(μ-Carboxylato) Cores. *J. Am. Chem. Soc.* **1988**, *110*, 1986.
(36) Bossek, U.; Weyhermüller, T.; Wieghardt, K.; Bonvoisin, J.; Girerd, J. J. Synthesis, e.s.r. Spectrum and Magnetic Properties of a Heterobinuclear Complex Containing the $\{Fe^{III}(\mu\text{-}O)(\mu\text{-}MeCO_2)_2Mn^{III}\}^{2+}$ Core. *J. Chem. Soc., Chem. Commun.* **1989**, 633−636.
(37) Das, B.; Daver, H.; Singh, A.; Singh, R.; Haukka, M.; Demeshko, S.; Meyer, F.; Lisensky, G.; Jarenmark, M.; Himo, F.; Nordlander, E. A Heterobimetallic $Fe^{III}Mn^{II}$ Complex of an Unsymmetrical Dinucleating Ligand: A Structural and Functional Model Complex for the Active Site of Purple Acid Phosphatase of Sweet Potato. *Eur. J. Inorg. Chem.* **2014**, *2014*, 2204−2212.
(38) Tereniak, S. J.; Carlson, R. K.; Clouston, L. J.; Young, V. G.; Bill, E.; Maurice, R.; Chen, Y.-S.; Kim, H. J.; Gagliardi, L.; Lu, C. C. Role of the Metal in the Bonding and Properties of Bimetallic Complexes Involving Manganese, Iron, and Cobalt. *J. Am. Chem. Soc.* **2014**, *136*, 1842−1855.
(39) Kerber, W. D.; Goheen, J. T.; Perez, K. A.; Siegler, M. A. Enhanced Stability of the $Fe^{II}/Mn^{II}$ State in a Synthetic Model of Heterobimetallic Cofactor Assembly. *Inorg. Chem.* **2016**, *55*, 848−857.
(40) Sano, Y.; Lau, N.; Weitz, A. C.; Ziller, J. W.; Hendrich, M. P.; Borovik, A. S. Models for Unsymmetrical Active Sites in Metalloproteins: Structural, Redox, and Magnetic Properties of Bimetallic Complexes with $M^{II}$-(μ-OH)-$Fe^{III}$ Cores. *Inorg. Chem.* **2017**, *56*, 14118−14128.
(41) Crossland, P. M.; Guo, Y.; Que, L., Jr. Spontaneous Formation of an Fe/Mn Diamond Core: Models for the Fe/Mn Sites in Class 1c Ribonucleotide Reductases. *Inorg. Chem.* **2021**, *60*, 8710−8721.
(42) Buchanan, R. M.; Mashuta, M. S.; Richardson, J. F.; Webb, R. J.; Oberhausen, K. J.; Nanny, M. A.; Hendrickson, D. N. Synthesis, Structure, and Properties of a Novel Heterobimetallic $Iron^{III}Manganese^{II}$ Complex Containing a Septadentate Polyimidazole Ligand. *Inorg. Chem.* **1990**, *29*, 1299−1301.
(43) Hotzelmann, R.; Wieghardt, K.; Floerke, U.; Haupt, H. J.; Weatherburn, D. C.; Bonvoisin, J.; Blondin, G.; Girerd, J. J. Spin Exchange Coupling in Asymmetric Heterodinuclear Complexes Containing the μ-Oxo-Bis(μ-Acetato)Dimetal Core. *J. Am. Chem. Soc.* **1992**, *114*, 1681−1696.
(44) Holman, T. R.; Wang, Z.; Hendrich, M. P.; Que, L. Structural and Spectroscopic Properties of Antiferromagnetically Coupled $Fe^{III}Mn^{II}$ and $Fe^{II}Mn^{II}$ Complexes. *Inorg. Chem.* **1995**, *34*, 134−139.
(45) Karsten, P.; Neves, A.; Bortoluzzi, A. J.; Lanznaster, M.; Drago, V. Synthesis, Structure, Properties, and Phosphatase-Like Activity of the First Heterodinuclear $Fe^{III}Mn^{II}$ Complex with the Unsymmetric Ligand $H_2$BPBPMP as a Model for the PAP in Sweet Potato. *Inorg. Chem.* **2002**, *41*, 4624−4626.
(46) Ross, S.; Weyhermüller, T.; Bill, E.; Bothe, E.; Flörke, U.; Wieghardt, K.; Chaudhuri, P. Asymmetric Heterodinuclear $Fe^{III}M^{II}$ (M = Zn, Cu, Ni, Fe, Mn), $Co^{III}Fe^{II}$ and $Fe^{II}Co^{III}$ Species: Synthesis, Structure, Redox Behavior, and Magnetism. *Eur. J. Inorg. Chem.* **2004**, *5*, 984−997.
(47) Jarenmark, M.; Haukka, M.; Demeshko, S.; Tuczek, F.; Zuppiroli, L.; Meyer, F.; Nordlander, E. Synthesis, Characterization, and Reactivity Studies of Heterodinuclear Complexes Modeling Active Sites in Purple Acid Phospatases. *Inorg. Chem.* **2011**, *50*, 3866−3887.
(48) Carboni, M.; Clémancey, M.; Molton, F.; Pécaut, J.; Lebrun, C.; Dubois, L.; Blondin, G.; Latour, J.-M. Biologically Relevant Heterodinuclear Iron−Manganese Complexes. *Inorg. Chem.* **2012**, *51*, 10447−10460.
(49) Sano, Y.; Weitz, A. C.; Ziller, J. W.; Hendrich, M. P.; Borovik, A. S. Unsymmetrical Bimetallic Complexes with $M^{II}$-(μ-OH)-$M^{III}$ Cores ($M^{II}M^{III}$ = $Fe^{II}Fe^{III}$, $Mn^{II}Fe^{III}$, $Mn^{II}Mn^{III}$): Structural, Magnetic, and Redox Prope. *Inorg. Chem.* **2013**, *52*, 10229−10231.
(50) Tao, W.; Bower, J. K.; Moore, C. E.; Zhang, S. Dicopper M-oxo, M-nitrosyl Complex from the Activation of NO or Nitrite at a Dicopper Center. *J. Am. Chem. Soc.* **2019**, *141*, 10159−10164.
(51) Tuttle, M. R.; Walter, C.; Brackman, E.; Moore, C. E.; Espe, M.; Rasik, C.; Adams, P.; Zhang, S. Redox-Active Zinc Thiolates for Low-Cost Rechargeable Aqueous Zn-Ion Batteries. *Chem. Sci.* **2021**, *12*, 15253−15262.
(52) LeCloux, D. D.; Barrios, A. M.; Mizoguchi, T. J.; Lippard, S. J. Modeling the Diiron Centers of Non-Heme Iron Enzymes. Preparation of Sterically Hindered Diiron(II) Tetracarboxylate Complexes and Their Reactions with Dioxygen. *J. Am. Chem. Soc.* **1998**, *120*, 9001−9014.
(53) He, C.; Lippard, S. J. Synthesis and Electrochemical Studies of Diiron Complexes of 1,8-Naphthyridine-Based Dinucleating Ligands to Model Features of the Active Sites of Non-Heme Diiron Enzymes. *Inorg. Chem.* **2001**, *40*, 1414−1420.
(54) Do, L. H.; Lippard, S. J. Toward Functional Carboxylate-Bridged Diiron Protein Mimics: Achieving Structural Stability and Conformational Flexibility Using a Macrocylic Ligand Framework. *J. Am. Chem. Soc.* **2011**, *133*, 10568−10581.
(55) Burger, B.; Dechert, S.; Große, C.; Demeshko, S.; Meyer, F. Visualising the Carboxylate Shift at a Bioinspired Diiron(II) Site in the Solid State. *Chem. Commun.* **2011**, *47*, 10428−10430.
(56) Minier, M. A.; Lippard, S. J. $^{19}F$ NMR Study of Ligand Dynamics in Carboxylate-Bridged Diiron(II) Complexes Supported by a Macrocyclic Ligand. *Dalton Trans.* **2015**, *44*, 18111−18121.
(57) Wang, F.; Becker, S.; Minier, M. A.; Loas, A.; Jackson, M. N.; Lippard, S. J. Tuning the Diiron Core Geometry in Carboxylate-Bridged Macrocyclic Model Complexes Affects Their Redox Properties and Supports Oxidation Chemistry. *Inorg. Chem.* **2017**, *56*, 11050−11058.
(58) Barynin, V. V.; Whittaker, M. M.; Antonyuk, S. V.; Lamzin, V. S.; Harrison, P. M.; Artymiuk, P. J.; Whittaker, J. W. Crystal Structure of Manganese Catalase from Lactobacillus Plantarum. *Structure* **2001**, *9*, 725−738.
(59) Bertini, I.; Turano, P.; Vila, A. J. Nuclear Magnetic Resonance of Paramagnetic Metalloproteins. *Chem. Rev.* **2002**, *93*, 2833−2932.
(60) Freedman, D. E.; Han, T. H.; Prodi, A.; Müller, P.; Huang, Q. Z.; Chen, Y. S.; Webb, S. M.; Lee, Y. S.; McQueen, T. M.; Nocera, D. G. Site Specific X-Ray Anomalous Dispersion of the Geometrically Frustrated Kagomé Magnet, Herbertsmithite, $ZnCu_3(OH)_6Cl_2$. *J. Am. Chem. Soc.* **2010**, *132*, 16185−16190.
(61) Powers, T. M.; Gu, N. X.; Fout, A. R.; Baldwin, A. M.; Hernández Sánchez, R.; Alfonso, D. M.; Chen, Y. S.; Zheng, S. L.; Betley, T. A. Synthesis of Open-Shell, Bimetallic Mn/Fe Trinuclear Clusters. *J. Am. Chem. Soc.* **2013**, *135*, 14448−14458.
(62) Garino, C.; Borfecchia, E.; Gobetto, R.; van Bokhoven, J. A.; Lamberti, C. Determination of the Electronic and Structural Configuration of Coordination Compounds by Synchrotron-Radiation Techniques. *Coord. Chem. Rev.* **2014**, *277−278*, 130−186.


https://doi.org/10.1021/jacs.2c11930
J. Am. Chem. Soc. 2023, 145, 3491−3498